

# A FE Procedure for Foundation Design of Offshore Structures – Applied to Study a Potential OWT Monopile Foundation in the Korean Western Sea

H.P. Jostad<sup>1</sup>, G. Grimstad<sup>2</sup>, K.H. Andersen<sup>3</sup>, M. Saue<sup>4</sup>, Y. Shin<sup>5</sup>, and D. You<sup>6</sup>

<sup>1</sup>Norwegian Geotechnical Institute, NGI, Oslo, Norway

<sup>2</sup>Norwegian University for Science and Technology, NTNU, Trondheim, Norway

<sup>4</sup>NGI Inc., Houston, Texas, USA

<sup>6</sup>GS Engineering & Construction Corp., Seoul, South Korea

E-mail: hpj@ngi.no

**ABSTRACT:** A finite element based calculation procedure that accounts for the effect of cyclic loading of soils under undrained conditions is presented. A material model called UDCAM that uses 3D strain contour diagrams from undrained cyclic and monotonic triaxial and DSS tests is used in the procedure. The model accounts for cyclic degradation by using the cyclic strain accumulation procedure developed at NGI in the seventies. The load history is idealized by a load composition containing load parcels with constant average and cyclic loads in each parcel. The applicability of the procedure is verified by back calculating a model test of a gravity base structure (GBS) in soft clay subjected to monotonic and cyclic loading. The procedure is then used to predict the behaviour of a monopile for a potential offshore wind turbine (OWT) in the Korean Western Sea. These results are compared with results obtained with traditional beam-spring analyses.

**KEYWORDS:** Offshore Engineering, Numerical modelling, Soil/structure interaction, Cyclic Loading, Clays, Monopiles, Wind Turbines

## 1. INTRODUCTION

Offshore wind turbine (OWT) structures are subjected to a combination of cyclic wind and wave loading. These loads together with the weight of the OWT and its equipment need to be carried by the soil without causing a foundation failure in the ultimate limit state (ULS) or unacceptable displacements and rotation in the serviceability limit state (SLS). In addition, the soil stiffness and damping will generally influence the dynamic behaviour of the OWT structure, including the natural frequencies and the dynamic amplification factor, and thus the fatigue limit state (FLS) of the structure.

Undrained cyclic loading of water saturated soil will generally reduce the shear stiffness and the undrained shear strength of the soil. NGI has during the last 30 years developed a framework to characterize and define the soil behaviour under cyclic loading (e.g. Andersen et al., 1988; Andersen, 2009), as well as calculation procedures (e.g. Andersen and Lauritzen, 1988, Andersen and Hoeg, 1991, Andersen, 1991) based on this framework. These procedures have been verified by several model tests, e.g. Andersen et al. (1989 and 1993), Keaveny et al. (1994), and used in the design of a large number of offshore structures such as gravity base structures, e.g. Brent B, Troll A and Gullfaks C, tension leg platforms, e.g. Heidrun and Snorre, and suction anchors for mooring of floating structures all around the world (Andersen et al., 2005).

In finite element (FE) analyses, cyclic soil models that seem to work fine in time domain for some few regular cycles tend to accumulate errors with increasing number of cycles and more irregular load histories. When hundreds or thousands of cycles are applied, the accuracy of such models is questionable. In addition, such models still require significant computational time and cost.

In this paper a description of a FE based procedure for undrained cyclic accumulation is presented. The model, which is called UDCAM (Undrained Cyclic Accumulation Model), accounts for degradation under undrained cyclic loading using the strain accumulation principle developed at NGI (Andersen et al., 1976). Instead of analyzing the cyclic load history in the time domain (implicit method), it considers the behaviour during application of the loads in so-called load parcels of constant average and cyclic load amplitudes (explicit method). The model then finds the reduced cyclic stiffnesses and accumulated permanent strains as described in this paper. At large strains, the calculated stresses are limited by anisotropic undrained cyclic shear strength. This model is implemented into the commercial finite element code Plaxis 3D

Foundation (Brinkgreve et al., 2007). It should be recognized that some other models also account for cyclic loading by an explicit method, e.g. as the high cyclic accumulation model for sand (Niemunis et al., 2005) and the degradation stiffness model also for sand (Achmus et al., 2009).

The applicability of the presented procedure is verified by back calculating a model test of a gravity base structure (GBS) in soft clay subjected to monotonic and cyclic loading (Dyvik et al., 1989). Then, the procedure is used to predict the behaviour of a monopile for a potential OWT in the Korean Western Sea. These results are compared with results obtained with traditional beam-spring analyses using p-y and t-z curves based on American Petroleum Institute (API, 2011). The model is applicable also for other foundation types such as gravity base structures and skirted foundations or caissons subjected to undrained cyclic loading.

## 2. CURRENT INDUSTRY PRACTICE

Current industry practice for monopile is to calculate capacity and displacements by semi empirical methods based on beam column models with the soil support represented by so called p-y and/or t-z springs. However, some special studies have been performed using the finite element method.

### 2.1 Beam column method with p-y and t-z springs

In semi empirical methods based on beam column models the soil is represented by uncoupled, non-linear soil springs along the pile (e.g. McClelland and Focht, 1958; API, 2011). In some formulations, the p-y curves include post-peak softening in order to account for effects of cyclic loading (Matlock, 1970; API, 2011). The semi empirical method has been used for analyses of piles for many years and is a familiar tool for many geotechnical engineers. However, the method has a number of limitations. It is based on empiricism from a limited amount of model tests on small piles. Therefore, it does not consider the severity of cyclic loading (e.g. variation in the cyclic load history) or that the cyclic behaviour depends on the soil type, other than grouping the soil into a few different soil types (soft clay, hard clay and sand). It does not account for the initial stiffness of the soil (dynamic stiffness) at small displacements or unloading/reloading cycles. It ignores coupling between the soil springs along the pile, which may be especially important for layered soils and short piles. It also ignores the coupling between horizontal and vertical soil springs. Further, it does not include independent side shear resistance components at the pile interface

on active and passive sides to model contribution to the moment resistance. In addition, it does not properly model effects of interface roughness and gradually loss of contact on the windward side. Finally, the method requires special springs to model rotational, vertical and horizontal tip resistance. These springs are also coupled with the p-y and t-z springs some distance above the pile tip.

Beam column methods where the soil support is represented by springs may, however, be a practical way to represent the soil in structural analyses. One should then consider establishing site and load specific springs by means of finite element analyses. An alternative is to define the interface between the foundation and the structural model at the seabed and to establish the coupled non-linear vertical, horizontal and rotational spring stiffness of the foundation at sea bed. These can then be used as input to a structural model starting at seabed. This alternative method is generally used for other types of offshore structures such as gravity base structures (GBS), jackets and jack-up platforms.

**2.2 The finite element method**

During the last decade it has become more common to use the finite element method in the design of offshore structures as for instance described in Andresen et al. (2010). At NGI, displacements and capacities have for instance been calculated based on stress-strain curves that assume a ratio between cyclic and average shear stresses throughout the soil volume equal to the ratio between cyclic and average load components for a constant equivalent number of cycles  $N_{eq}$  of the peak cyclic loads (e.g. Andersen and Hoeg, 1991). For plane-strain conditions, the displacements and capacity may be calculated by the procedure described in Jostad and Andresen (2009) where strain compatibility under both average and cyclic loads is found by an iterative procedure. The actual shear stress – shear strain relationship in each integration point is derived from cyclic contour diagrams for a given  $N_{eq}$ . Descriptions of cyclic contour diagrams are given in Section 3.1. However, the assumption of a constant  $N_{eq}$  may underestimate the effect of stress redistribution and progressive failure due to large cyclic degradation in stiffnesses and strengths. Furthermore, the extension to general 3D stress states and redistribution of average and cyclic shear stresses due to a spatial variation in the cyclic degradation were necessary in order to be able to perform appropriate analyses of monopile foundations for OWT structures.

**3. CALCULATION PROCEDURE**

The calculation procedure presented here is based the same philosophy as used in the past at NGI for considering the behaviour of soil subjected to combined undrained static and cyclic loading. However, in the present procedure all calculations are integrated into a finite element based procedure using a material model called UDCAM (Undrained Cyclic Accumulation Model). Compared to the formulation presented in Jostad and Andresen (2009), the present procedure includes the extension to the full 3D state and calculation of cyclic degradation in each integration point based on the actual shear stress history in each point. The main input to the procedure is an idealized cyclic load composition and 3D cyclic contour diagrams as described in the following.

**3.1 Cyclic contour diagrams**

The behaviour of soil subjected to undrained cyclic loading is at NGI established from stress controlled undrained cyclic and monotonic triaxial and direct simple shear (DSS) tests. Since the cyclic behaviour of soil, different from other materials as for instance steel, generally is highly dependent on the average shear stress level, the cyclic shear stress (amplitude)  $\tau_{cy}$  is in the cyclic tests applied together with a constant average shear stress  $\tau_a$ . The measured response during the cyclic tests is then the development of

the average shear strain  $\gamma_a$  and the cyclic shear strain (amplitude)  $\gamma_{cy}$  as function of the number of cycles  $N$ , see Figure 1.

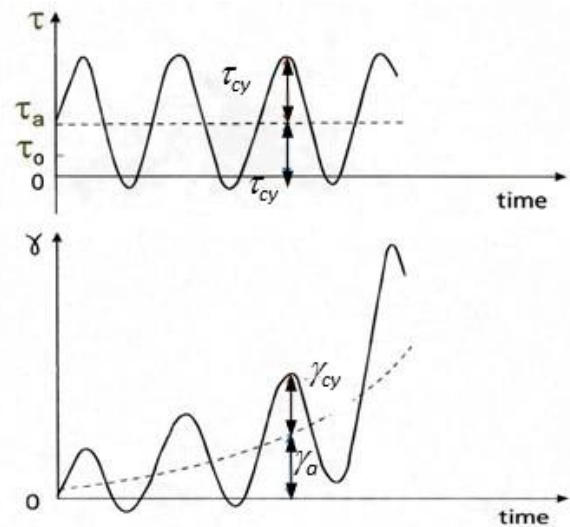


Figure 1 Development of average and cyclic shear strains with increasing number of cycles in a soil element subjected to combined average and cyclic shear stresses

Instead of fitting the behaviour of advanced constitutive models developed for cyclic loading to the measured responses (since it generally becomes too inaccurate), the non-linear relationships between average shear stress  $\tau_a$ , cyclic shear stress  $\tau_{cy}$ , average shear strain  $\gamma_a$ , cyclic shear strain  $\gamma_{cy}$  and number of cycles  $N$  are traditionally at NGI represented by so-called cyclic contour diagrams. Example of a full 3D diagram, given as cross sections for  $N = 1, 10, 100$  and  $400$ , for DSS stress states is shown in Figure 2.

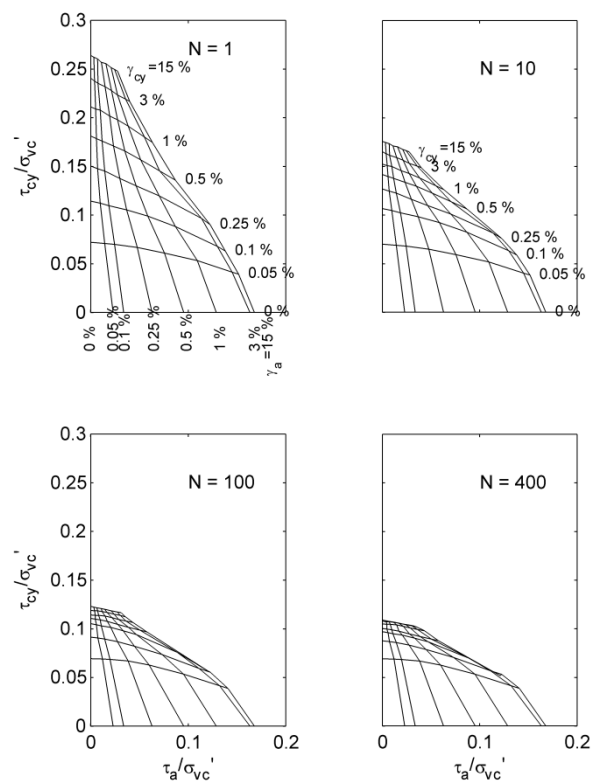


Figure 2 Example of 3D contour diagram (cross sections at constant  $N$ ) for DSS conditions, the strain contour values are the same for all cross sections of  $N$

The boundaries of the diagram give the cyclic shear strength, i.e. combination of average and cyclic shear stresses at large average or cyclic shear strains as function of the number of cycles. At NGI we generally use a shear strain of 15% to define failure. The average and cyclic shear stresses in the example are normalized by the effective vertical (consolidation) stress,  $\sigma_{vc}'$ , before the undrained tests. However, other suitable de-normalisation stresses may be used as for instance the undrained triaxial compression shear strength,  $s_u^C$ . The de-normalisation should make the diagram valid for a given soil layer.

The advantage of establishing these diagrams is that the results from a limiting number of laboratory tests are interpolated and extrapolated in the stress space in a controllable way, using experiences from tests on other similar soils. Further explanation of how these contour diagrams are established is given in Andersen (2009). However, in the future the cyclic diagrams will most likely instead be represented by some kind of mathematical frameworks, which also may partly be based on a constitutive framework. In the meanwhile, the diagrams are digitized by tables of sampling points  $(\tau_a, \tau_{cy}, \gamma_a, \gamma_{cy}, N)_k$ , and simple interpolation methods are used between these points. In order to obtain one variable from a diagram you need input of 3 variables, where one of the variables is either a consistent stress or strain value.

### 3.1.1 General 3D stress state

In order to transfer these characteristic stress states given by the contour diagrams, to a general 3D stress state, a simple interpolation is used between the triaxial, where the axial stresses and strains are assumed to coincide with the vertical axis, and the DSS stress state. In lack of other more advanced laboratory tests (with possibility to apply more general stress states), it is assumed that the DSS stress state is representative for the remaining stress states not covered by the triaxial state. The contribution of triaxial behaviour is then calculated as the ratio between the vertical deviatoric strain and a proper deviatoric strain invariant representing the total shear strain level. The shear stress for a general principal stress orientation is then found by an elliptic interpolation function between the triaxial stress state and the DSS stress state. A slightly different interpolation function between these states has previously been presented for an elastoplastic anisotropic shear strength model in Grimstad et al. (2012). The cartesian stress components are found by assuming coaxiality between the principal strains and the principal stresses. This is solved by first calculating the orientations of the principal strains. Then calculating principal deviatoric stresses based on the shear stress found by interpolating between triaxial and DSS stress states and the angle of the intermediate principal deviatoric strain. Finally, adding the mean stress and transforming the principal stresses back to the actual coordinate system. The mathematical formulation of this process is shown in the Appendix. How the same transformation was solved in 2D was presented in Jostad and Andresen (2009).

### 3.2 Cyclic load composition

Instead of applying a time load history to the FE model, it is found to be more convenient (especially in cases where the load history consists of a large number of load cycles) to consider the behaviour during application of the loads in so-called load parcels. The load parcels are then an idealized load composition where the load history is divided into numbers of constant cyclic load amplitudes around a constant average load within each load parcel as illustrated in Figure 3.

To establish this load composition one may for instance use the rain flow method (Matsuishi and Endo, 1968), which generally is used to establish the design load compositions for the fatigue limit state (FLS) of steel components subjected to cyclic loading. However, to better represent the cyclic load history that accounts for the characteristic behaviour of soil subjected to undrained cyclic loading, NGI is currently studying other methods for counting the number of cycles at different cyclic load levels around a continuously varying average load.

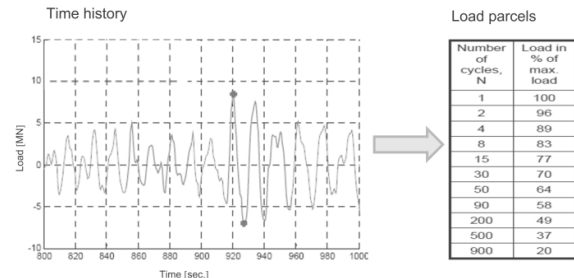


Figure 3 Transformation of cyclic load history (only part of the total time history is shown) to load parcels with constant cyclic load and zero average load in this case

In order to determine the cyclic degradation of the soil, the effect of the experienced cyclic loading history is represented by calculation of an equivalent number of cycles  $N_{eq}$  at the current cyclic shear stress level. The procedure uses the cyclic shear strain  $\gamma_{cy}$  as a state parameter to determine  $N_{eq}$  from a contour diagram, as described in Andersen (1976).

### 3.3 Calculation phases

Due to the coupling between the average and the cyclic shear stress-shear strain relationships as shown by the cyclic contour diagrams, it is necessary to perform the analyses by a semi coupled procedure. Therefore, the analysis for a given load parcel is divided into three phases: (1) Application of average loads  $F_a$ ; (2) Application of cyclic loads  $F_{cy}$ ; and (3) Input of the number of cycles  $\Delta N$  at the given load level. The average or cyclic material behaviour are updated between each phase (without any iteration between the phases). The average phase will produce output of  $\tau_a$  and  $\gamma_a$ , in each integration point, as a function of  $N_{eq}$ ,  $\gamma_{cy}$  and  $F_a$ . The cyclic phase gives output of  $\gamma_{cy}$ ,  $\tau_{cy}$  and  $N_{eq}$  as a function of  $\gamma_a$ ,  $F_{cy}$  and  $\Delta N$ . The third phase is only used for specifying the number of new cycles  $\Delta N$ . This procedure (except phase 3) is similar to the procedure proposed by Jostad and Andresen (2009) for redistribution of stresses due to average and cyclic loading in plane strain analyses with a predetermined constant  $N_{eq}$ .

### 3.4 Simple example calculation

In order to illustrate how the calculation procedure works, a hypothetical cyclic DSS test has been simulated. The material behaviour is given by the contour diagram in Figure 2. Five cyclic load parcels with zero average horizontal shear stress according to Table 1 are applied. The calculated  $N_{eq}$  after each parcel is given in the last row of the same table. Figure 4 shows the calculated cyclic shear stress - strain relationship during the applied load composition. The plateaus represent the increase in cyclic shear strain with number of cycles under the constant cyclic shear stress amplitude. In Figure 5 the history of how  $N_{eq}$  and  $\gamma_{cy}$  change during application of the load parcels is illustrated in the cross section of  $\tau_{cy}$  versus  $N$  with contours of  $\gamma_{cy}$  (DSS condition with  $\gamma_a$  and  $\tau_a$  of zero). The circles represent the calculated cyclic shear strain at beginning and end of each load parcel. The procedure includes the direct increase in cyclic shear stress amplitude when increasing the cyclic shear

stress level as explained in more details in Andersen (1976) and Andersen et al. (1992).

Table 1 Load application scheme for the cyclic DSS simulation

Parcel	1	2	3	4	5
$\tau_{cy}/s_u^C$	0.458	0.498	0.531	0.571	0.598
$\Delta N$	15	8	4	2	1
Calculated $N_{eq}$	15	15	13	10	8

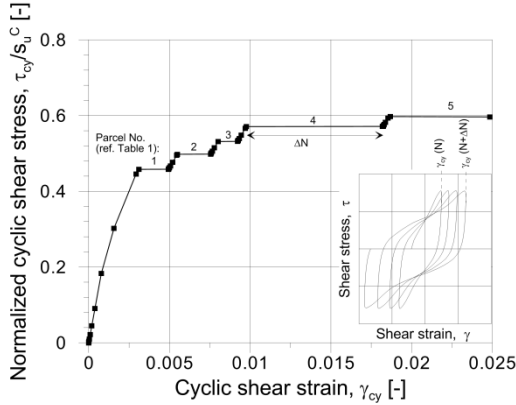


Figure 4 Cyclic stress-strain curve obtained from the FE simulation of a hypothetical DSS test

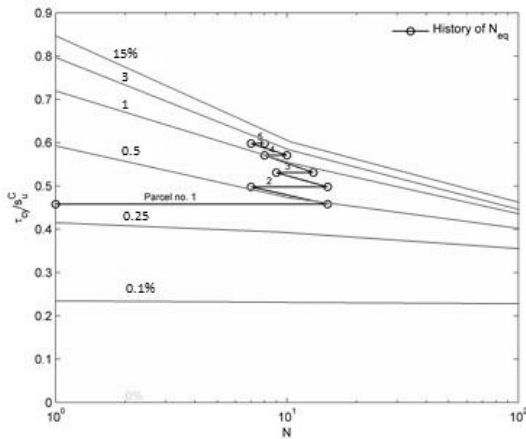


Figure 5 History of obtained  $N_{eq}$  in a cross section with  $\tau_a = 0$  of a DSS cyclic shear strain contour diagram

4. VERIFICATION CALCULATIONS

To verify the design of the foundation of the GBS at the Troll field offshore Norway, a series of model tests were performed. The clay properties, the model geometry, the test program, and the test results are described in Dyvik et al. (1989). The following interpretation and back calculation of the tests are presented in Andersen et al. (1989). Jostad and Andresen (2009) present FEM analyses of the model tests using the NGI procedure with a predetermined  $N_{eq}$ , equal for the entire soil volume. Only cross sections of the DSS and triaxial contour diagrams at this  $N_{eq}$  were then used as input to this FEM analysis. Results from back-calculation of the same model test with both 2D and 3D FE models using the new developed calculation procedure, are presented here. The main differences in the new analyses are the calculation of  $N_{eq}$  in each integration point after each load parcel and the extension to the general 3D stress state in the soil.

The model test was performed with a circular foundation with a diameter 0.4 m and skirts that were penetrated 0.095 m into the clay. The bin with clay had a diameter of 1.0 m and a depth of 0.2 m. The

submerged weight of the structure was 2.825 kN and the horizontal load was applied 0.4 m above the clay surface. The clay in the bin was reconstituted Mowm clay with a consolidated vertical effective stress of 36 kPa + 100 kPa/m [depth below clay surface], which gives a monotonic undrained triaxial compression shear strength profile of  $s_u^C = 0.27 \cdot \sigma_{vc}' = 10 \text{ kPa} + 27 \text{ kPa/m}$  (i.e. increasing from 10 kPa at the clay surface to 15 kPa at the bottom of the bin). The clay was not consolidated under the weight of the model. Normalized contour diagrams are given in Andersen et al. (1989). However, extrapolations to  $N = 1$  and  $N = 400$  were in this study done based on the DSS cross section. Figure 6 and Figure 7 give the contour diagrams for Mowm Clay as used in the analyses, for triaxial and DSS state, respectively.

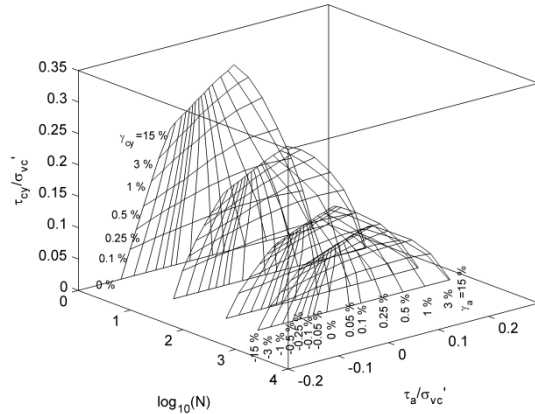


Figure 6 Contour diagram for triaxial state for Mowm clay

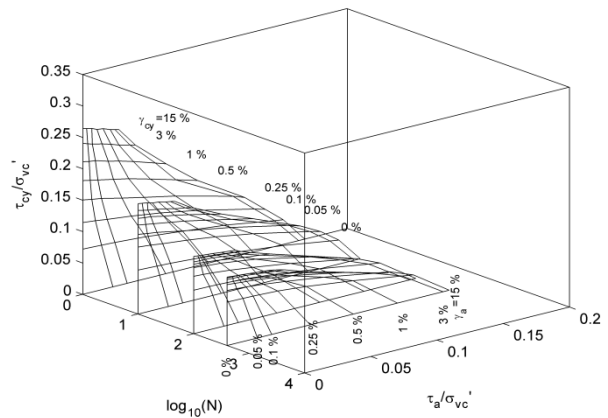


Figure 7 Contour diagram for DSS state for Mowm clay

The cyclic load history that was applied in the considered test (Test 2 in Dyvik et al. 1989) is here transferred into suitable load parcels, as given in Table 2. The parcels are given with increasing cyclic horizontal loads, except for the final load parcel, where the load was reduced. The average horizontal load is zero. Andersen et al. (1989) found that the  $N_{eq}$  after the last parcel was 38, when assuming a shear stress response proportional to the applied horizontal cyclic loads. Therefore, an analysis in 2D with  $N_{eq} = 40$  (close enough to 38) for all integration points is done to see if the calculated cyclic capacity (for  $N_{eq} = 40$ ) is similar to the measured. This will verify that the new procedure also can reproduce the expected capacity using the original calculation procedure. The idealized 2D FE geometry is modelled by a plane strain foundation with an equivalent width of 0.346 m. As can be seen in Figure 8, the calculated capacity of the foundation using the new procedure with constant  $N$ , agrees well with the measured response. The same 2D model has also been used in an analysis where the cyclic load

history has been applied in load parcels. The result is presented in Figure 9. The result for this case compare well with the analysis with a constant  $N_{eq}$ .

The 3D model used in Plaxis 3D Foundation, see Figure 10, did not have the same refined discretization as the 2D model, in order to reduce the calculation time. Therefore, it has been assumed that the analyses of cyclic and monotonic tests have the same discretization error. The cyclic results are then presented as values normalized with respect to the calculated monotonic capacity. The 3D model consists of 6552, 15 noded wedge elements, while the 2D analyses were run with 598, 15 noded triangular elements. In all cases the foundation was modelled with a stiff elastic material, such that significant deformation of the foundation was avoided. In Figure 9 the 3D and the 2D simulations are compared to the measured response in terms of horizontal displacement of the foundation at clay surface level. The 3D and the 2D analyses compare well in terms of calculated normalized cyclic capacity. Andersen et al. (1989) calculated that  $N_{eq}$  at the maximum cyclic load was 14 or alternatively  $\log_{10}(N_{eq}) = 1.146$ . The calculated  $\log_{10}(N_{eq})$  for cyclic shear strain above 1.0% (effectively in the zone where the failure mechanism is located) is found to be between 1.1 and 1.2. This means that the 3D finite element calculation with UDCAM gives the same  $N_{eq}$  within the failure zone, at the peak load, as found by the original procedure in Andersen et al. (1989).

Table 2 Cyclic load series for the considered test (Test 2)

Parcel	1	2	3	4	5	6	8	9	10	11	13
$N$	15	10	7	4	3	20	10	7	4	1	20
$H_{cy}$ [N]	240	480	510	537	575	601	660	709	761	808	719
$V_a$	W	W	W	W	W	W	W	W	W	W	W

W = 2.825 kN

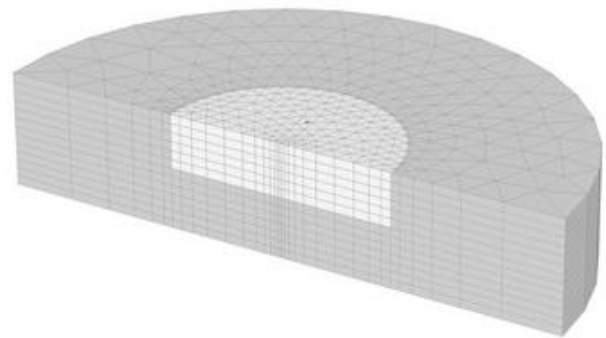


Figure 10 FE model of the GBS model foundation

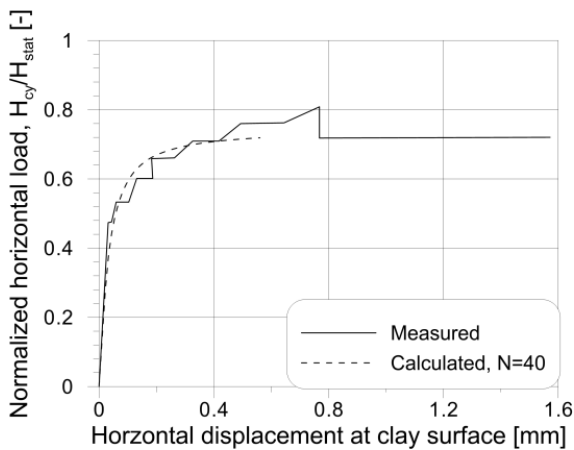


Figure 8 Horizontal load – displacement curve for the 2D simulation, with constant  $N_{eq} = 40$ , compared to measured response

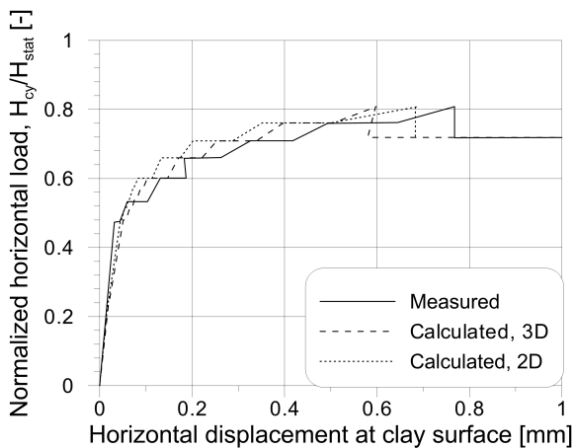


Figure 9 Normalized horizontal load – displacement curve for the 3D simulation compared to measured response and 2D simulation

### 5. CASE STUDY

As part of a study of different foundation types applicable for offshore wind turbines in the Korean Western Sea the presented FE procedure using the new material model UDCAM was used to analyse an alternative with a monopile foundation. The obtained results are then compared with results obtained with the beam column method using cyclic  $p$ - $y$  curves (API, 2011).

The considered monopile is a tubular steel pile with a diameter of 5.2 m, penetration depth of 45 m and constant wall thickness of 54 mm, which supports a 3 MW wind turbine. Characteristic design loads and general soil properties, including index and strength parameters, are from an actual wind farm pilot site currently under development in the Korean Western Sea. The soil conditions typically consist of alternating layers of close to normally consolidated silty clay to silt and loose silty sand. In this case study soil properties for the silty clay to silt are used as input to all layers in the analyses.

Both the ultimate limit state (ULS) and the serviceability limit state (SLS) are evaluated using load and material factors according to DNV (2010). For the ULS case a load factor of 1.35 is applied to the environmental loads, and a material factor of 1.25 has been used to reduce the undrained shear strengths. Twenty-four different Design Load Cases (DLCs) were evaluated in accordance with the IEC (2007) for the monopile structure. The most critical resultant characteristic loads at seabed are summarized in Table 3. Load histories were in this phase of the project in lack of an established composition for an OWT structure, based on a typical North Sea storm composition for a GBS (Andersen, 1991). This composition is most likely different for an OWT structure, however, the authors believe that the composition represents a possible scenario for the extremes of a storm dominated by wave loads. Constant height of the resultant horizontal force  $H$  above seabed, i.e.  $M/H$  ratio, and constant vertical load  $V$ , and constant average  $M$  and  $H$  equal to 20% of the peak loads are assumed throughout the storm. The storm composition is shown in Figure 11.

Table 3 Characteristic resultant ULS loads at seabed (DLC 14)

Overturning moment, M	159 175	kNm
Horizontal load component, H	4 231	kN
Vertical load component, V	9 104	kN

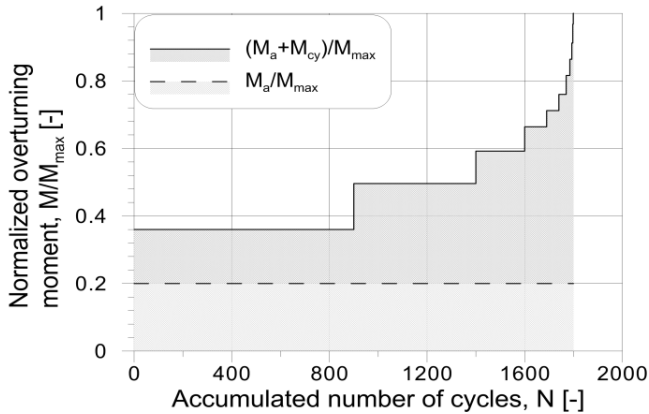


Figure 11 Load history applied in FE analyses of the OWT monopile foundation

In order to derive relevant input data for the soil at the pilot site some limited laboratory tests were performed on intact specimens. The laboratory program consisted of index tests, constant rate of strain oedometer tests, and monotonic and cyclic constant volume DSS tests. The index properties vary somewhat within the soil unit. However, typical values for the material tested are summarized in Table 4.

Table 4 Index properties for the Korean Western Sea silty clay to silt

Initial water content, w	30 %
Total unit weight, $\gamma$	18 kN/m <sup>3</sup>
Plasticity Index, $I_p$	13 %
Clay content	12 %
Fines content (grain size < 0.06 mm)	70-80 %

The monotonic DSS tests show a normalized static undrained direct simple shear strength  $s_u^{DSS}/\sigma'_{vo}$  of about 0.35. Anisotropy undrained shear strength ratios of  $s_u^{DSS}/s_u^C = 0.90$  and  $s_u^E/s_u^C$  of 0.45 are based on laboratory tests on similar types of silty clay. Data from similar soils were also utilised in order to establish appropriate cyclic properties. The cyclic 3D contour diagrams that were applied are presented in Figure 12 for the triaxial state and Figure 13 for the DSS state.

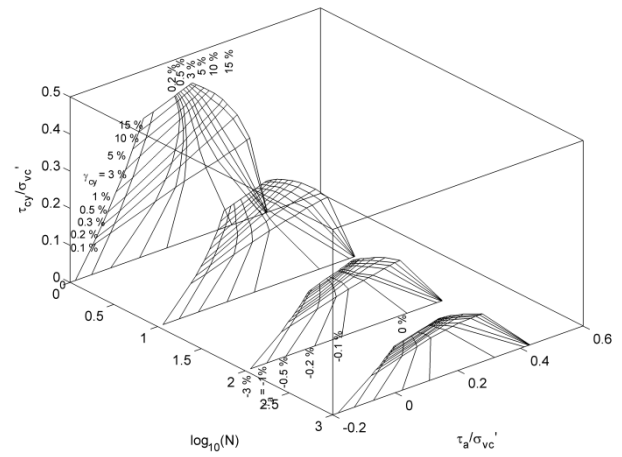


Figure 12 Contour diagram for triaxial state for the clay at the West Korean site

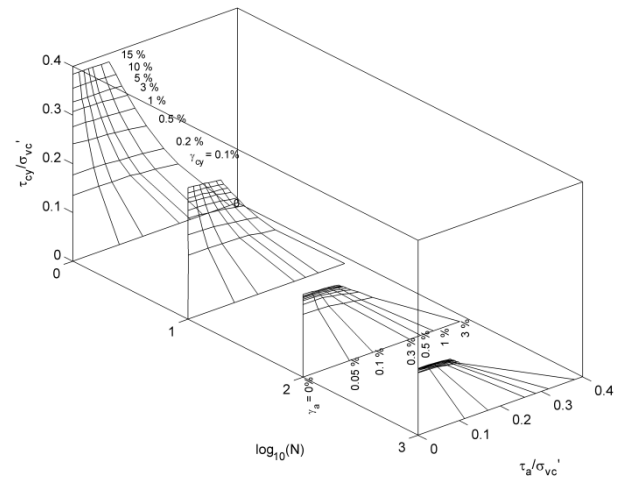


Figure 13 Contour diagrams for DSS state for the clay at the West Korean site

In the beam column analyses the unconfined undrained compression strength,  $s_u^{UU}$ , is for simplicity assumed to be equal to  $s_u^{DSS}$  and the strain parameter  $\epsilon_{50}$ , that controls the stiffness, is modelled according to values given in Matlock (1970). Furthermore, a dimensionless J-factor of 0.5 was applied in the analyses.

The calculations were performed with both a finite difference beam-column code with the API (2011) cyclic p-y curves and Plaxis 3D Foundation Version 2.2 (Brinkgreve, 2007) with UDCAM as a user-defined material model. The finite element model used in the analyses is presented in Figure 14. A mesh discretization study showed that the mesh used in the calculations gives an estimated overshoot in capacity of about 4 %.

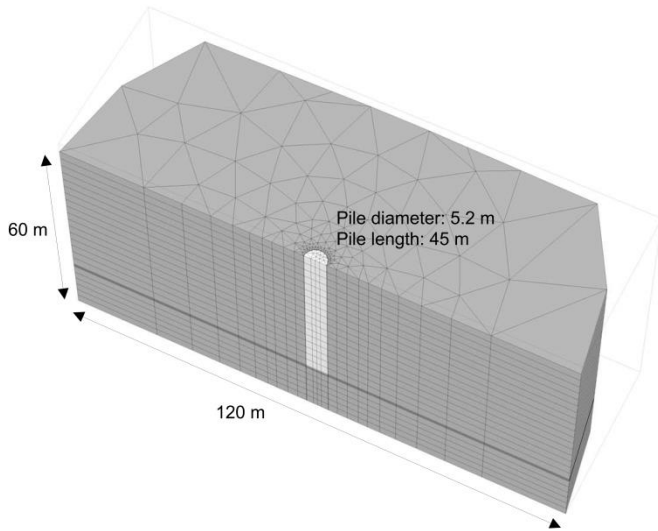


Figure 14 FE model of the monopile foundation

Figure 15 presents the calculated cyclic shear strain in the soil at the end of the applied ULS load history. The figure shows that the largest soil mobilization occurs in the upper part of the soil close to the monopile. Figure 16 shows a plot of  $\log_{10}(N_{eq})$  for the ULS condition in the area with cyclic shear strain larger than 0.1%. As it can be seen in the figure,  $N_{eq}$  is highest towards the top of the soil profile. The combination of a high  $N_{eq}$  and large cyclic stresses results in the largest cyclic degradation and thereby a reduction in soil resistance.

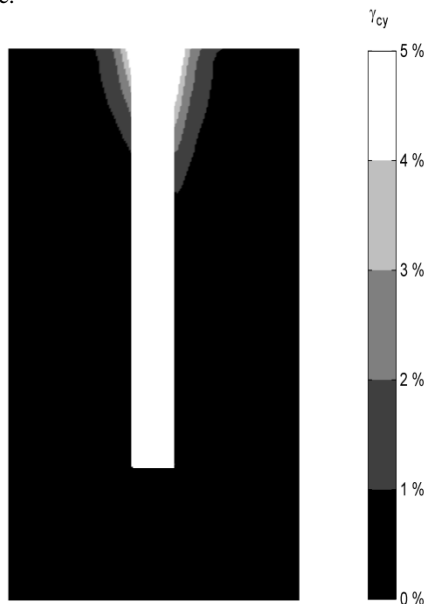


Figure 15 Contour plot of calculated cyclic shear strain in ULS condition

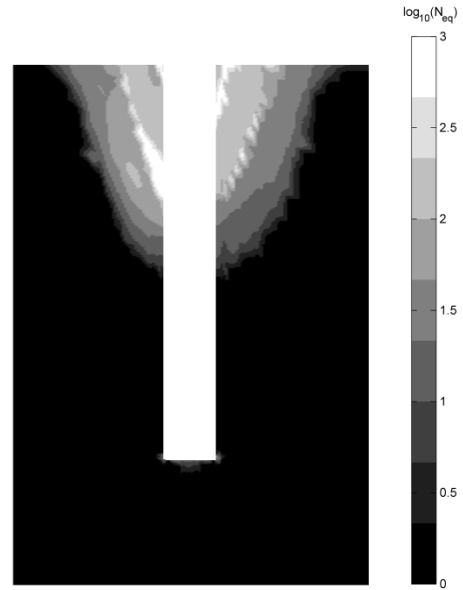


Figure 16 Contour plot of calculated  $\log_{10}(N_{eq})$  at the symmetry plane for the ULS condition in the area with cyclic shear strain larger than 0.1%

Figure 17 and Figure 18 present results from the beam-spring analyses together with results from the FE analyses for the ULS and SLS cases, respectively. The beam-spring analyses are done with different assumptions with respect to the base shear resistance. One case assumes no base shear resistance. The other case assume that the base shear resistance is  $s_u^{DSS} \cdot A$ , where  $A$  is the base area. The mobilization of the base shear is assumed to follow the API p-y curves. It is found that the base shear has a minor effect on the result in this specific case.

Horizontal pile displacement, rotation, bending moment, shear force, normalized soil resistance and soil reactions along the pile are presented. The obtained results are very different for the two calculation methods, both for the SLS and the ULS conditions. It is seen that the pile is likely to be close to failure ( $\sim 0.4$ m) for the ULS load when using the beam-spring approach, while the FE analysis only gives a maximum pile displacement of 0.2 m. Similarly, it is seen that the rotation of the pile top for the SLS condition is reduced from more than 0.61 degrees using the beam-spring approach with no base shear, to 0.45 degrees in the FE analysis. Design requirements are often related to both the capacity in ULS and the rotation of the pile top in SLS. This implies that FE analyses of a shorter pile may give a more optimized design. It is also seen that the bending moments and shear forces in the pile are larger and appear at greater depth when using the beam-spring approach which may also result in a too conservative design.

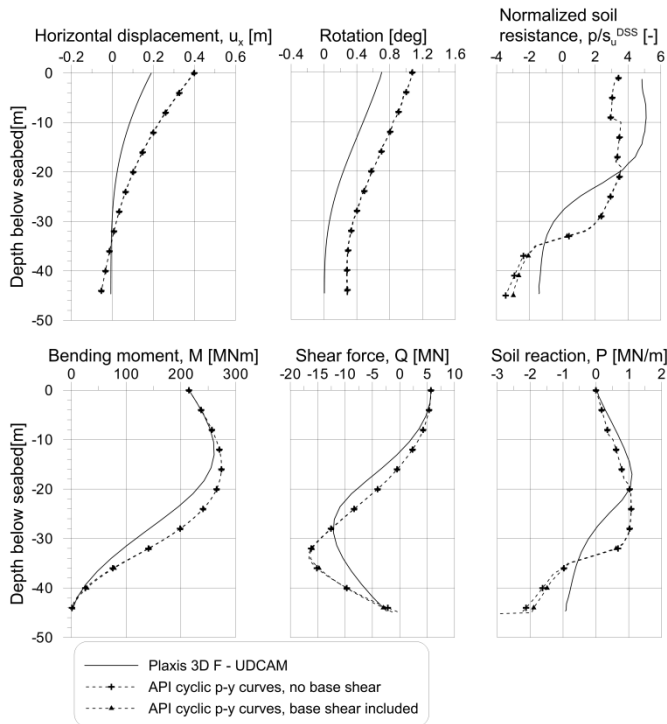


Figure 17 Results from beam-spring and Plaxis 3D Foundation (UDCAM) calculations, ULS

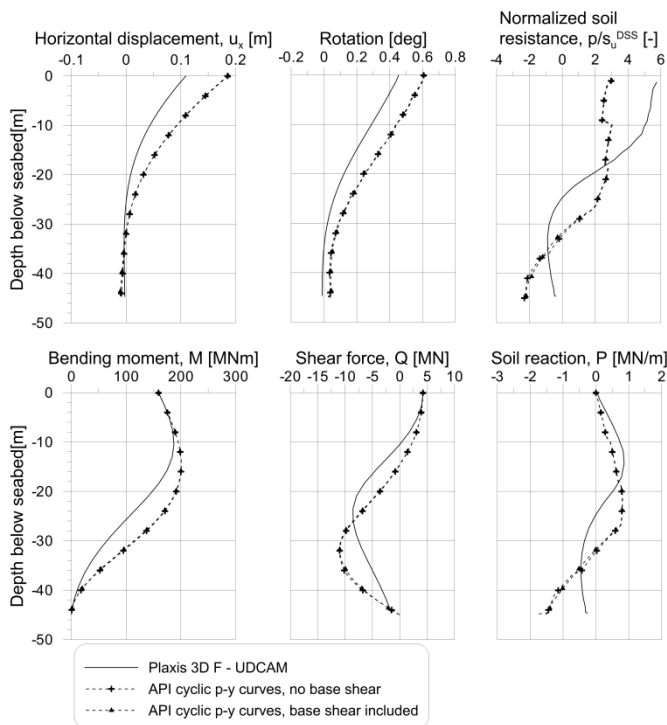


Figure 18 Results from beam-spring and Plaxis 3D Foundation (UDCAM) calculations, SLS

There are several reasons for the difference in the results between the beam-spring and the FE analyses. These are related both to the way the soil is modelled and to the methodology applied. As stated in Section 2.1, the beam-spring approach includes several simplifications, and it is believed that these limitations are largely responsible for the differences. One reason for the difference seen in this case study, is that the API p-y curves for a soft clay with  $s_u \leq 100$  kPa, include an ultimate resistance,  $P_u$ , increasing from about

$3 \cdot s_u^{UU} \cdot D$  at seabed to a maximum of  $9 \cdot s_u^{UU} \cdot D$  at greater depth. The increase in  $P_u$  with depth is highly dependent on the depth-diameter ratio of the pile. For cyclic p-y curves,  $P_u$  is even smaller since the shear strength is reduced by a factor of more than 0.72 due to cyclic degradation since these curves also include further reduction at large displacements (softening). These values are low compared to FE results which typically include a maximum lateral monotonic resistance of 9 to 12  $\cdot s_u^{DSS} \cdot D$  for depths where lateral flow-around the pile occurs. However, cyclic degradation may reduce this maximum value. The normalized soil resistance  $p/s_u^{DSS}$  presented in Figure 17 shows the effect of this difference directly. While the beam-spring analysis shows a value starting from about  $3 \cdot 0.72 = 2.2$  at seabed and only minor increase with depth, the FE analyses show values between 4 to 5.5 in the upper 15 m. The beam-spring approach will then need to utilize soil resistance deeper down along the pile, which is also seen in Figure 17. When comparing the ULS and the SLS results from the FE analyses, it is seen that the soil resistance in the top 10 m is smaller for the ULS case than for the SLS case. This is due to larger degradation of the soil strength in the upper 10 m for the ULS case.

In both the beam-spring and the finite element analyses it is important to model a possible gap between the soil and the pile on the windward side. The effect of a gap is accounted for in the empirically based API p-y curves. In the FE analyses presented herein this effect is included by preventing any tension stresses in excess of the hydrostatic water pressure between the pile and soil by including a thin zone around the pile with a material with a total stress based tension cut-off criterion. Development of the gap during cyclic loading is however a very complex mechanism, with free water flowing in and out of the gap with potential erosion. Further research is required in order to address this in an appropriate way.

## 6. CONCLUSIONS

A finite element based calculation procedure that accounts for the effect of cyclic loading in undrained conditions has been presented. A material model called UDCAM that uses 3D cyclic contour diagrams for undrained triaxial and DSS stress states as input is developed at NGI. The model accounts for cyclic degradation in the integration points by calculating the equivalent number of cycles using the cyclic strain accumulation procedure developed at NGI. The procedure analyses the considered cyclic load history by applying several load parcels with constant average and cyclic loads within each load parcel. The procedure is much more time efficient and robust than models following each cycle, especially when a large number of cycles is considered. The results of monotonic and cyclic laboratory tests are part of the input data. Therefore, these tests will automatically be reproduced by the model. The procedure has been verified by back-calculating the behaviour of a GBS model test on soft clay subjected to cyclic loading. This back-calculation demonstrates that the model is able to produce results that agree well with the measurements. The last part of the paper demonstrates that the procedure is well suited for cases where the cyclic degradation varies within the soil mass, such as for monopile foundations for offshore wind turbines. The obtained results indicate that the use of the traditional beam spring approach together with API cyclic p-y curves could be too conservative for this type of large diameter stiff piles in low permeable soils.

## 7. ACKNOWLEDGMENTS

The presented work was performed as a joined project between GS E&C Research Institute in South Korea and Norwegian Geotechnical Institute (NGI). The implementation of the user-defined UDCAM model into a FE code was financed by GS E&C. The procedures presented in this paper are based on previous joint industry-sponsored research projects, research projects funded by the Research Council of Norway, and consulting projects.

### 8. APPENDIX

From the strain vector (either average or cyclic) an equivalent shear strain,  $\gamma_{eq}$  and two measures of strain rotations are calculated. To create the  $\gamma_{eq}$  the angle for intermediate principal strain,  $\theta$ , and the variable for the contribution of triaxial strain  $X$  are calculated with the corresponding transformation matrix,  $\mathbf{a}$ , and strain invariants  $\varepsilon_{oct}$  and  $J_{2e}$ . Equations (2) to (6) define how the strain measures are calculated. Equation (1) defines the transformation matrix,  $\mathbf{a}$ , and the principal deviatoric strains  $e_1$ ,  $e_2$  and  $e_3$ . The principal normal strains  $\varepsilon_1$ ,  $\varepsilon_2$  and  $\varepsilon_3$  are found from an eigenvalue calculation. Note that in the present formulation it is assumed that the vertical axis is the y-axis as it is in Plaxis 3D Foundation.

$$\begin{bmatrix} e_1 + \varepsilon_{oct} & 0 & 0 \\ 0 & e_2 + \varepsilon_{oct} & 0 \\ 0 & 0 & e_3 + \varepsilon_{oct} \end{bmatrix} = \mathbf{a} \cdot \boldsymbol{\varepsilon} \cdot \mathbf{a}^T \quad (1)$$

where:

$$\varepsilon_{oct} = tr(\boldsymbol{\varepsilon})/3 \quad (2)$$

$$\gamma_{eq} = e_1 - e_3 \quad (3)$$

$$\theta = \text{asin}(e_2 / \sqrt{J_{2e}} \cdot \sqrt{3} / 2) \quad (4)$$

where:

$$J_{2e} = -e_1 e_2 - e_2 e_3 - e_1 e_3 \quad (5)$$

$$X = e_y / \sqrt{J_{2e}} \cdot \sqrt{3} / 2 \quad (6)$$

For a given maximum shear strain(average or cyclic)  $\gamma_{eq}$ , three shear stresses are obtained from the contour diagrams,  $\tau_{TXC}$ ,  $\tau_{DSS}$  and  $\tau_{TXE}$ , being the shear stress in triaxial compression, DSS and triaxial extension, respectively. The shear stresses can be average or cyclic, depending on the calculation mode.

If the stress is cyclic, then  $\tau_{TXE} = -\tau_{TXC}$ . The equivalent isotropic shear stress,  $\tau$ , is then defined according to equation (7) assuming a simple elliptic interpolation function between the triaxial and DSS stress state.

$$\tau = \frac{1}{2} \cdot \sqrt{(\tau_{TXC} - \tau_{TXE})^2 \cdot X^2 + 4 \cdot \tau_{DSS}^2 \cdot (1 - X^2)} \quad (7)$$

The mean stress at increment,  $p$ , is calculated by:  $p = K \cdot 3 \cdot \Delta\varepsilon_{oct}$ , where  $K$  is the bulk stiffness. For undrained conditions  $K$  is taken as a numerical high value that gives negligible volumetric strains. The deviatoric principal stresses,  $s_1$ ,  $s_2$  and  $s_3$ , are calculated as given in equations (8) to (10) below:

$$s_1 = \tau \cdot \left(1 - \frac{1}{\sqrt{3}} \cdot \tan \theta\right) \quad (8)$$

$$s_2 = \frac{2}{\sqrt{3}} \cdot \tau \cdot \tan \theta \quad (9)$$

$$s_3 = -\tau \cdot \left(1 + \frac{1}{\sqrt{3}} \cdot \tan \theta\right) \quad (10)$$

From these principal deviatoric stresses the Cartesian stress tensor is established as (equation 11):

$$\boldsymbol{\sigma} = \mathbf{a}^T \cdot \begin{bmatrix} s_1 & 0 & 0 \\ 0 & s_2 & 0 \\ 0 & 0 & s_3 \end{bmatrix} \cdot \mathbf{a} + p \cdot \mathbf{I} + \frac{1}{3} (\tau_{TXC} + \tau_{TXE}) \cdot \begin{bmatrix} -1 & 0 & 0 \\ 0 & 2 & 0 \\ 0 & 0 & -1 \end{bmatrix} \quad (11)$$

### 9. REFERENCES

Achmus, M., Kuo, Y-S., Abdel-Rahman, K. (2009). Behaviour of monopole foundations under cyclic lateral load. *Computers and Geotechnics* 36, 725-735.

Andersen, K.H. (1976). Behaviour of clay subjected to undrained cyclic loading. *Proc. 1st Int. Conf. on the Behaviour of Offshore Structures, BOSS'76, Trondheim 1*, 392-403.

Andersen, K. H., Kleven, A., and Heien, D. (1988). Cyclic soil data for design of gravity structures. *J. Geotech. Engrg., ASCE*, 114, 517-539.

Andersen, K.H. and Lauritzen, R. (1988). Bearing capacity for foundation design with cyclic loads. *J. Geotech. Engrg., ASCE*, 114, 540-555.

Andersen, K.H., Dyvik R., Lauritzen, R., Heien, D., Hårvik, L., Amundsen, T. (1989). Model tests on gravity platforms. II: Interpretation. *J. Geotech. Engrg., ASCE*, 115, 1550-1568.

Andersen, K.H. (1991). Foundation design of offshore gravity structures. Chapter 4 in "Cyclic Loading of Soils. From Theory to Design". Edited by M.P. O'Reilly and S.F. Brown. Publ. by Blackie and Son Ltd., Glasgow and London, pp.122-173.

Andersen, K.H. and Hoeg, K. (1991) Deformations of soils and displacements of structures subjected to combined static and cyclic loads. *Proc. 10th Eur. Conf. Soil Mech., Florence 4*, 1147-1158.

Andersen, K.H., Dyvik, R., Kikuchi, Y., Skomedal, E. (1992). Clay behaviour under irregular cyclic loading. *Proc. 6th Int. Conf. on the Behaviour of Offshore Structures, London 2*, 937-950.

Andersen, K.H., Dyvik R., Schrøder K., Hansteen O.E and Bysveen S. (1993). "Field tests of anchors in clay II: Predictions and interpretation". *J. Geotech. Engrg., ASCE*, 119, pp. 1532-1549.

Andersen, K.H. (2004). Cyclic data for foundation design of structures subjected to wave loading. *Proc. of Conf. on cyclic behaviour of soils and liquefaction phenomena, Bochum, Germany. CRC Press, Taylor & Francis Group, London* pp. 371-387.

Andersen, K.H., Murff, J.D., Randolph, M.F., Clukey, E., Erbrich, C., Jostad, H.P., Hansen, B., Aubeny, C., Sharma, P. and Supachawarote, C. (2005). "Suction anchors for deepwater applications." Keynote Lecture. *Proceedings, ISFOG, International Symposium on Frontiers in Offshore Geotechniques. 19-21 September, 2005. Perth, Western Australia.*

Andersen, K.H. (2009). Bearing capacity under cyclic loading - offshore along the coast, and on land. The 21st Bjerrum Lecture presented in Oslo, 23 November 2007. *Canadian Geotechnical Journal*, 45, No. 2, 513-535.

Andresen, L., Jostad, H. P. and Andersen, K. H. (2010). Finite Element Analyses Applied in Design of Foundations and Anchors for Offshore Structures. *International Journal of Geomechanics*, doi:10.1061/(ASCE)GM.1943-5622.0000020.

API (2011), American Petroleum Institute, *Geotechnical and Foundation Design Considerations*. ANSI/API RP 2GEO, 1th Edition, Washington, April 2011.

DNV 2010. DNV-OS-J101, *Design of Offshore Wind Turbine Structures*, October 2010.

- Dyvik, R., Andersen, K.H., Madshus, C. and Amundsen, T. (1989). Model tests on gravity platforms. I: Description. J. Geotech. Engrg., ASCE, 115, 1532-1549.
- Grimstad, G., Andresen, L. and Jostad, H. P. (2012). NGI ADP: Anisotropic Shear Strength Model for Clay, Journal for Numerical and Analytical Methods in Geomechanics, 36, 483-497, doi: 10.1002/nag.1016.
- IEC (2007), International Electrotechnical Commission, Wind turbines, Part 1: Design Requirements, IEC 61400-1. 3<sup>rd</sup> edition, 2007.
- Jostad, H.P. and Andresen L. (2009). A FE procedure for calculation of displacements and Capacity of foundations subjected to cyclic loading. Proceedings for COMGEO I, Juan-les-Pins, Cote d'Azur, France.
- Jostad, H.P., Andersen, K.H., Tjelta, T.I. (1997). Analyses of skirted foundations and anchors in sand subjected to cyclic loading. Proceedings for International Conference on the Behaviour of Offshore Structures, 8. Delft, The Netherlands, . 1, 49-162. Also publ in: Norwegian Geotechnical Institute, Oslo. Publication, 199.
- Keaveny, J.M., Hansen J.B., Madshus C. and Dyvik R. (1994). "Horizontal capacity of large scale model anchors". XIII ICSMFE, New Delhi, Proc., Vol. 2, pp. 677-680.
- Matlock, H. (1970). Correlations for design of laterally loaded piles in soft clay. Proc. Offshore Technology Conference, Houston, 1, 577-594.
- McClelland, B. and Focht, J. (1958). Soil Modulus for Laterally Loaded Piles. Transactions, ASCE, 123, 1049-1086.
- Matsuishi, M. & Endo, T. (1968) Fatigue of metals subjected to varying stress, Japan Soc. Mech. Engineering.
- Niemunis, A, Wichtmann, T, Triantafyllidis, T., 2005. A high-cycle accumulation model for sand. Computers and Geotechnics; 32. No. 4, 245-263.

$\gamma_a^{TX}$	average shear strain in triaxial compression
$\gamma_a^{DSS}$	average shear strain in direct simple shear
$\gamma_{cy}$	cyclic shear strain [%]
$\gamma_{eq}$	equivalent shear strain
$\Delta$	increment
$\theta$	angle for intermediate principal strain
$\sigma$	Cartesian stress tensor
$\sigma'_{vo}$	vertical effective overburden stress
$\sigma'_{vc}$	vertical preconsolidation stress
$\tau$	shear stress [kN/m <sup>2</sup> ]
$\tau_a$	average shear stress [kN/m <sup>2</sup> ]
$\tau_{cy}$	cyclic shear stress [kN/m <sup>2</sup> ]
$\tau_{TXC}$	shear stress in triaxial compression [kN/m <sup>2</sup> ]
$\tau_{TXE}$	shear stress in triaxial extension [kN/m <sup>2</sup> ]
$\tau_{DSS}$	shear stress in direct simple shear [kN/m <sup>2</sup> ]
$X$	variable for amount of triaxial state of strain

## 10. LIST OF NOTATION

$A$	area of pile footprint [m]
$\mathbf{a}$	transformation matrix
$D$	pile diameter [m]
$e_y$	vertical deviatoric strain component ( $\epsilon_y - \epsilon_{oct}$ )
$e_{1,2,3}$	principal deviatoric strains
$\mathbf{F}$	load vector
$\mathbf{F}_a$	average load vector
$\mathbf{F}_{cy}$	cyclic load vector
$H_{cy}$	cyclic horizontal load [kN]
$H_{stat}$	horizontal load at static failure [kN]
$J$	dimensionless factor used in API p-y curves [-]
$J_{2\epsilon}$	second deviatoric invariant of strain
$K$	bulk stiffness
$M_a$	average moment [kNm]
$M_{cy}$	cyclic moment [kNm]
$M_{max}$	maximum applied moment ( $M_{cy} + M_a$ ) <sub>max</sub> [kNm]
$N$	number of cycles [-]
$N_{eq}$	equivalent number of cycles [-]
$P$	soil resistance [kN/m]
$p$	soil resistance normalized on diameter [kN/m <sup>2</sup> ]
$P_u$	ultimate soil resistance [kN/m]
$s_{1,2,3}$	principal deviatoric stresses
$s_u^c$	undrained shear strength in triaxial compression [kN/m <sup>2</sup> ]
$s_u^{DSS}$	undrained shear strength in direct simple shear [kN/m <sup>2</sup> ]
$s_u^E$	undrained shear strength in triaxial extension [kN/m <sup>2</sup> ]
$s_u^{UU}$	unconsolidated undrained shear strength in triaxial compression [kN/m <sup>2</sup> ]
$V_a$	average vertical load [kN]
$\epsilon$	Cartesian strain tensor
$\epsilon_{50}$	at half the maximum stress on laboratory unconsolidated undrained compression tests of undisturbed soil samples
$\epsilon_{oct}$	octahedral normal strain
$\gamma_a$	average shear strain [%]